

## Creating Complex Optical Longitudinal Polarization Structures

F. Maucher,<sup>1,2</sup> S. Skupin,<sup>3,4</sup> S. A. Gardiner,<sup>1</sup> and I. G. Hughes<sup>1</sup>

<sup>1</sup>*Joint Quantum Centre (JQC) Durham-Newcastle, Department of Physics, Durham University, Durham DH1 3LE, United Kingdom*

<sup>2</sup>*Department of Mathematical Sciences, Durham University, Durham DH1 3LE, United Kingdom*

<sup>3</sup>*Univ. Bordeaux—CNRS—CEA, Centre Lasers Intenses et Applications, UMR 5107, F-33405 Talence, France*

<sup>4</sup>*Institut Lumière Matière, UMR5306 Université Lyon 1 - CNRS, Université de Lyon, F-69622, Villeurbanne, France*



(Received 12 January 2018; published 16 April 2018)

In this Letter, we show that it is possible to structure the longitudinal polarization component of light. We illustrate our approach by demonstrating linked and knotted longitudinal vortex lines acquired upon nonparaxially propagating a tightly focused subwavelength beam. The remaining degrees of freedom in the transverse polarization components can be exploited to generate customized topological vector beams.

DOI: [10.1103/PhysRevLett.120.163903](https://doi.org/10.1103/PhysRevLett.120.163903)

The concept of light being a transverse wave—that is, the direction of the electric field is perpendicular to the propagation direction defined by the Poynting flux—represents an approximation that is suitable if the angular spectrum is sufficiently narrow [1]. However, many practical applications ranging from microscopy to data storage require tight focusing. Tight focusing implies a broad angular spectrum, and the notion of light being transverse becomes inappropriate. Hence, the longitudinal polarization component can typically not be neglected [2,3]. Here, longitudinal polarization refers to the electric field component parallel to the propagation direction, and transverse polarizations to the ones perpendicular to the latter. To mention a few examples, a “needle beam” with a particularly large longitudinal component was proposed in Ref. [4], and radial transverse polarization permits the significant decrease of the focal spot size [5,6], while the generated longitudinal component may even dominate the interaction with matter [7]. Last but not least, a Möbius strip in the polarization of light was realized in Ref. [8].

In addition, there is current substantial interest in “structured light,” that is, generating customized light fields that suit specific needs in applications in a range of fields [9–14]. Since the proposal of the Gerchberg-Saxton algorithm [15] in 1972, advances in light shaping [16–18] now permit the realization of complex light patterns in the transverse polarization plane, including light distributions, the optical vortex lines [19] of which form knots [20–23]. Knotted topological defect lines and their dynamics have been studied in diverse other settings, including, for example, classical fluid dynamics [24–26], excitable media [27–29], and nematic colloids [30,31]. To date, the approach has typically been to determine the longitudinal polarization component of the electric field from given transverse components [2,32], and attempts to target complex structures in the longitudinal component have not yet been pursued. The reason for this is twofold. On the one

hand, the longitudinal component is not directly accessible by beam-shaping techniques. On the other hand, nonparaxial beam configurations are required, and topological light is usually studied in the paraxial approximation. It is therefore not immediately evident that the whole range of three-dimensional light configurations known for transverse components can be realized in the longitudinal component as well.

In this Letter, we will show that complex light shaping of the longitudinal polarization component is indeed possible. To this end, we first identify nonparaxial light patterns that give rise to vortex lines that form knots or links. Second, we invert the problem and derive how one must structure the transverse components of a tightly focused beam to give rise to a *given* complex pattern in the longitudinal component and, thus, present the first example of nontransverse nonparaxial knots. Finally, we demonstrate that the remaining degrees of freedom in the transverse polarization components allow for simultaneous transverse shaping, which could be interesting for applications, e.g., inscribing vortex lines into Bose-Einstein condensates.

We begin with the equations describing a monochromatic light beam:

$$\nabla^2 \mathbf{E}(\mathbf{r}_\perp, z) + k_0^2 \mathbf{E}(\mathbf{r}_\perp, z) = 0, \quad (1)$$

$$\nabla \cdot \mathbf{E}(\mathbf{r}_\perp, z) = \nabla_\perp \cdot \mathbf{E}_\perp + \partial_z E_z = 0. \quad (2)$$

Here,  $k_0^2 = \omega^2/c^2 = (2\pi/\lambda)^2$ , and we have introduced the transverse coordinates  $\mathbf{r}_\perp = (x, y)$  and transverse electric field components  $\mathbf{E}_\perp = (E_x, E_y)$  as we consider propagation in the positive  $z$  direction. All three components of  $\mathbf{E}$  in Eq. (1) fulfill the same wave equation, and for a given field configuration  $\mathbf{E}^f(\mathbf{r}_\perp)$  at  $z = 0$  (e.g., at focus) the general solution for propagation in the positive  $z$  direction reads  $\hat{\mathbf{E}}(\mathbf{k}_\perp, z) = \hat{\mathbf{E}}^f(\mathbf{k}_\perp) \exp(ik_z z)$ , where  $k_z(\mathbf{k}_\perp) = \sqrt{k_0^2 - \mathbf{k}_\perp^2}$ ,

$\mathbf{k}_\perp = (k_x, k_y)$ , and the symbol  $\hat{\cdot}$  denotes the transverse Fourier domain. The prescribed field configuration  $\hat{\mathbf{E}}^f$  must obey certain constraints. First, in order to get a valid bulk solution far away from any interfaces, there must be no evanescent fields present; that is,  $\hat{\mathbf{E}}^f = 0$  for  $\mathbf{k}_\perp^2 \geq k_0^2$ . Second, Eq. (2) implies for solutions propagating in the  $z$  direction that  $\hat{E}_z^f(\mathbf{k}_\perp = 0) = 0$ .

As preparation for what follows, we first investigate how to obtain a nonparaxial tightly focused knot or link in  $E_z$ , assuming that we can directly prescribe  $E_z^f$ . For the transverse paraxial case, recipes to generate vortex lines in various shapes are known, and they usually involve linear combinations of Laguerre-Gaussian modes [22,33]. These paraxial recipes are not directly applicable to our problem, since at such a small width the Laguerre-Gaussian modes contain a considerable amount of evanescent field amplitudes. Moreover, due to the nonparaxiality, the whole problem becomes wavelength dependent, and, as already mentioned above, we have to ensure that  $\hat{E}_z^f(\mathbf{k}_\perp = 0) = 0$ , as otherwise Eq. (2) would be violated. Nevertheless, we found that it is possible to adopt those recipes for the nonparaxial case by an educated guess. Starting from a given linear combination of Laguerre-Gaussian modes  $f$ , filtering in the transverse Fourier domain [34],

$$H_{k_0}(\mathbf{k}_\perp) = e^{-1/[2\lambda^2(\sqrt{k_\perp^2 - k_0^2})^2]}, \quad H_0(\mathbf{k}_\perp) = 1 - e^{-(3\lambda k_\perp)^2},$$

chops off evanescent amplitudes as well as amplitudes close to  $\mathbf{k}_\perp = 0$ , and the longitudinal polarization component at  $z = 0$  reads

$$\hat{E}_z^f(\mathbf{k}_\perp) = \begin{cases} \hat{f}(\mathbf{k}_\perp)H_{k_0}H_0 & \text{for } \mathbf{k}_\perp^2 < k_0^2, \\ 0 & \text{for } \mathbf{k}_\perp^2 \geq k_0^2. \end{cases} \quad (3)$$

Since the higher-order Laguerre-Gaussian modes are broader in Fourier space and thus lose relative weight after attenuation, one must decrease the relative amplitudes of the lower-order modes to a certain extent. We have found that the following field structures produce a Hopf link or trefoil, respectively:

$$f^{\text{Hopf}} = 4\text{LG}_{00}^\sigma - 5\text{LG}_{01}^\sigma + 11\text{LG}_{02}^\sigma - 8\text{LG}_{20}^\sigma, \quad (4)$$

$$f^{\text{trefoil}} = 9\text{LG}_{00}^\sigma - 20\text{LG}_{01}^\sigma + 40\text{LG}_{02}^\sigma - 18\text{LG}_{03}^\sigma - 34\text{LG}_{30}^\sigma, \quad (5)$$

for wavelength  $\lambda = 780$  nm and width  $\sigma = 370$  nm  $\approx \lambda/2$  of the usual Laguerre-Gaussian modes  $\text{LG}_{ij}^\sigma(\mathbf{r}_\perp)$ . The resulting amplitudes before and after filtering for  $f$  being either  $f^{\text{Hopf}}$  or  $f^{\text{trefoil}}$  defined in Eqs. (4) and (5) are plotted in Fig. 1 after normalization to unity. We note that individual mode amplitudes can be changed by about 10% without altering the topology, demonstrating a degree of robustness and hence experimental feasibility.

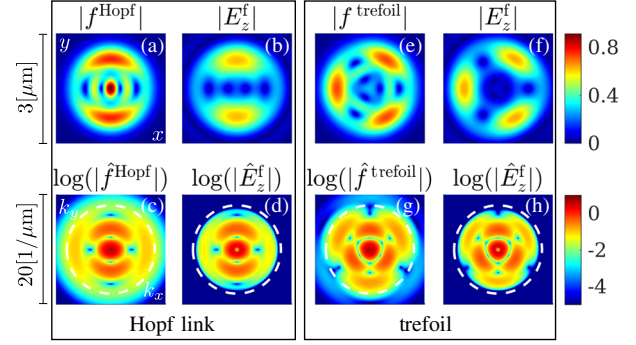


FIG. 1. The profiles  $f^{\text{Hopf}}$  and  $f^{\text{trefoil}}$  of Eqs. (4) and (5) (a),(e) at narrow widths contain evanescent waves. This is demonstrated in (c) and (g), where the profiles are shown in the transverse Fourier domain together with a circle of radius  $k_0$ . A spectral attenuation (d),(h) according to Eq. (3) removes the evanescent amplitudes as well as amplitudes close to  $\mathbf{k}_\perp = 0$  (see the text for details) and alters  $E_z^f$  in the focal plane significantly (b),(f).

Let us now verify that the presented patterns in the focal plane in fact give rise to vortex lines with the desired topology. It is straightforward to propagate the filtered component  $E_z^f$ , as defined in Eq. (3), in the  $z$  direction. The vortex lines throughout three-dimensional space are depicted by the black lines in Figs. 2(a) and 2(b) together with a slice in the  $z = 0$  plane of the light profile phase. The obtained vortex lines are topologically equivalent to a Hopf link and a trefoil, as drawn in the insets.

We now address the main point of this Letter, i.e., how to choose the transverse polarization components to obtain a given longitudinal polarization component. Because only the transverse components  $E_x$  and  $E_y$  are accessible to beam shaping, this point is also of great practical relevance. When inspecting Eq. (2), at first glance the problem may seem to be ill posed, given that only the longitudinal derivative of the longitudinal polarization enters, i.e.,  $\partial_z E_z$ . However, in Fourier space it is easy to see from Eq. (2) that a linearly polarized solution to this problem is given by

$$E_x^f = e^f = -i \int_{-\infty}^x \mathcal{F}^{-1}[k_z \hat{E}_z^f](x', y) dx', \quad E_y^f = 0, \quad (6)$$

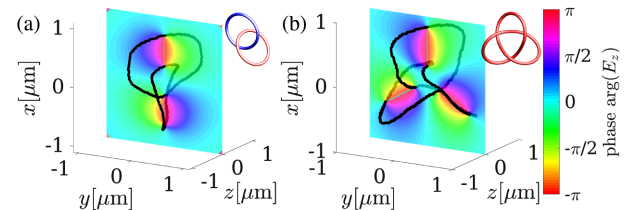


FIG. 2. Propagation of the spectrally attenuated field shown in Figs. 1(b) and 1(f) gives rise to the vortex lines (black) in the forms of a Hopf link (a) and a trefoil (b). A phase slice is shown in the  $xy$  plane at  $z = 0$ . As a comparison, the idealized Hopf link and trefoil are shown as insets.

where  $\mathcal{F}^{-1}[\hat{g}](x, y) = g(x, y)$  denotes the inverse transverse Fourier transformation. Obviously, an orthogonally polarized solution also exists:

$$E_x^f = 0, \quad E_y^f = e_y^f = -i \int_{-\infty}^y \mathcal{F}^{-1}[k_z \hat{E}_z^f](x, y') dy'. \quad (7)$$

Both  $x$ - and  $y$ -polarized solutions Eqs. (6) and (7) evaluated for a Hopf link and trefoil are depicted in Fig. 3. It is noteworthy that any superposition of real and imaginary parts of the solutions Eqs. (6) and (7) is admissible, as long as the coefficients of this superposition add up to one. Furthermore, any arbitrary field with zero longitudinal component could be added. We will discuss this later in more detail.

Unfortunately, the transverse polarization components computed from Eqs. (6) and (7) are impractical, since, even though  $E_z^f$  has finite support, the components  $E_x^f = e_x^f$  or  $E_y^f = e_y^f$  are nonzero on a semi-infinite interval (see Fig. 3). However, simply attenuating these components by multiplying with, e.g., a sufficiently wide super-Gaussian profile  $\text{SG}_N^w(\mathbf{r}_\perp) = \exp(-r_\perp^{2N}/w^{2N})$  allows the resolution of the problem of semi-infinite light distributions without affecting the propagation of the longitudinal component close to the optical axis. Evaluating  $\nabla_\perp \cdot [\text{SG}_N^w(\mathbf{r}_\perp) \mathbf{E}_\perp^f(\mathbf{r}_\perp)]$  reveals that, where  $\nabla_\perp \text{SG}_N^w$  is large and points in the direction of  $\mathbf{E}_\perp^f$ , additional satellite spots in the longitudinal component will appear. We have checked that using, e.g., a super-Gaussian with  $N = 5$  and  $w = 10\lambda$  ensures that these additional spots are sufficiently far from the region of interest and both the Hopf link and trefoil develop in the propagation of the modified  $E_z$  component.

So far, we have seen that the answer to the problem of how to choose  $\mathbf{E}_\perp^f(\mathbf{r}_\perp)$  for realizing a prescribed  $E_z^f$  is not

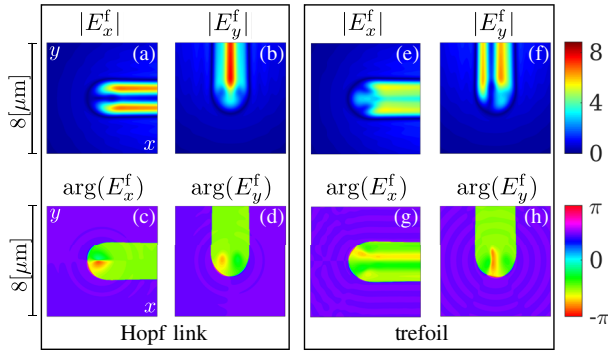


FIG. 3. Amplitude and phase in the  $z = 0$  plane for the linearly polarized transverse components Eqs. (6) and (7) that give rise to a longitudinal component forming the Hopf link [Figs. 1(b) and 2(a)] are shown in (a)–(d) and the trefoil [Figs. 1(f) and 2(b)] is shown in (e)–(h). The color maps for each figure are on the right of the two rows of plots. Both transverse fields  $\mathbf{E}_\perp^f = (e_x^f, 0)$  and  $\mathbf{E}_\perp^f = (0, e_y^f)$  shown in (a)–(d) and (e)–(h), respectively, yield the same longitudinal field, as well as superpositions  $\mathbf{E}_\perp^f = (\alpha e_x^f, \beta e_y^f)$  as long as the coefficients fulfill  $\alpha + \beta = 1$ .

unique, and there are certain degrees of freedom in the choice of  $\mathbf{E}_\perp^f$ . The fundamental theorem of vector calculus (Helmholtz decomposition) allows us to decompose a (sufficiently well-behaved) vector field  $\mathbf{F}$  into an irrotational (curl-free) and a solenoidal (divergence-free) vector field. In the three-dimensional version,  $\mathbf{F}$  can be written as  $\mathbf{F} = -\nabla\phi + \nabla \times \mathbf{A}$ , where  $\phi(\mathbf{r})$  and  $\mathbf{A}(\mathbf{r})$  are usually referred to as the scalar and vector potential, respectively. We wish to apply this theorem to the two-dimensional transverse plane ( $z = 0$ ) only; that is, we set  $\mathbf{F} = \mathbf{E}_\perp^f(\mathbf{r}_\perp)$ , and the decomposition reduces to

$$E_{\perp i}^f(\mathbf{r}_\perp) = -\partial_i V(\mathbf{r}_\perp) + \sum_j \varepsilon_{ij} \partial_j W(\mathbf{r}_\perp), \quad (8)$$

where  $i$  denotes one of the components ( $x, y$ ),  $\varepsilon_{ij}$  denotes the usual Levi-Civita symbol, and  $V(\mathbf{r}_\perp)$  and  $W(\mathbf{r}_\perp)$  denote scalar fields. The potentials  $V$  and  $W$  play analogue roles to  $\phi$  and  $\mathbf{A}$  in the standard three-dimensional situation mentioned above. For what is about to follow, it is important to note that the second term on the right-hand side of Eq. (8) is divergence-free in the two-dimensional transverse plane by construction, since  $\sum_{i,j} \partial_i \varepsilon_{ij} \partial_j W = 0$ .

Coming back to our initial question of how to choose  $\mathbf{E}_\perp^f$  in order to produce a desired  $E_z^f$ , it is straightforward to verify that

$$\hat{V}(\mathbf{k}_\perp) = -i \frac{k_z(\mathbf{k}_\perp) \hat{E}_z^f(\mathbf{k}_\perp)}{\mathbf{k}_\perp^2} \quad (9)$$

gives rise to a valid transverse polarization component  $\mathbf{E}_\perp^f$ . Then, the (sufficiently well-behaved) scalar function  $W(\mathbf{r}_\perp)$  may be chosen arbitrarily and does not give rise to any longitudinal polarization component. The irrotational choice for  $\mathbf{E}_\perp^f$ , that is, evaluating Eqs. (8) and (9) with  $W(\mathbf{r}_\perp) = 0$ , for the Hopf link and trefoil are shown in Fig. 4.

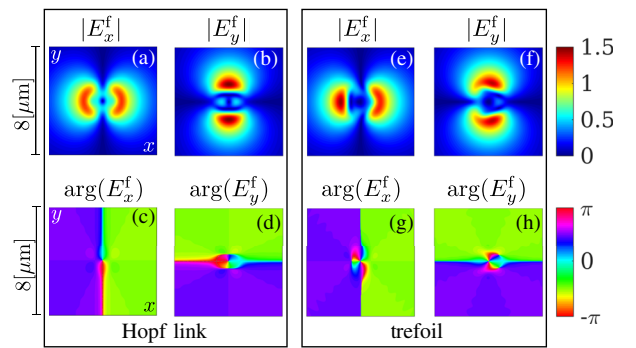


FIG. 4. Irrotational transverse amplitude and phase profiles in the  $z = 0$  plane producing a Hopf link (a)–(d) and a trefoil (e)–(h) in the longitudinal polarization component. In contrast to Fig. 3, here the transverse field producing the desired longitudinal component is fixed by Eqs. (8) and (9) to  $\mathbf{E}_\perp^f = -\nabla_\perp V(\mathbf{r}_\perp)$ , and we cannot change the weight of the components shown in (a)–(d) and (e)–(h), respectively.

While the transverse polarization components shown in Figs. 3 and 4 produce exactly the same longitudinal field, they are completely different, in particular, from a topological point of view. Unlike the light distributions in Fig. 3, which do not contain vortices in the transverse polarization components, the irrotational transverse polarization components in Fig. 4 each feature phase singularities. Furthermore, note that the amplitudes required in the irrotational transverse polarizations are only roughly 2–3 times the peak amplitude in the longitudinal polarization. Finally, in contrast to Eqs. (6) and (7), the irrotational choice Eqs. (8) and (9) with  $W(\mathbf{r}_\perp) = 0$  gives rise to a transverse light distribution with finite support, provided that the prescribed  $E_z^f(\mathbf{r}_\perp)$  has finite support.

We have seen that all possible transverse polarization components producing a certain longitudinal component differ by a two-dimensional solenoidal field ( $\partial_y W, -\partial_x W$ ), and the function  $W(\mathbf{r}_\perp)$  represents the degree of freedom one has when shaping the  $\mathbf{E}_\perp^f$ . As our examples show, it is possible to control the topological structure of longitudinal and transverse electric field components simultaneously. Tightly focused beams containing vortex lines could play a role in inscribing vortex lines with specific topology into Bose-Einstein condensates using two-photon Rabi transitions [33,35]. The demonstrated knotted or linked longitudinal vortex lines have an extent of roughly  $1 \mu\text{m}^3$  and thus match the typical size of a Bose-Einstein condensate. Being able to exploit the unique features of structured light in all three vector components of the electric field opens new avenues in controlling the interaction of light with matter.

An important practical issue is to actually experimentally detect such a small structure in the longitudinal polarization component. Probing of the longitudinal field using molecules was achieved experimentally roughly 15 years ago [36] and continues to be of interest for light-matter interactions [37]. We propose using a tomographic method using a thermal rubidium vapor cell that is very thin compared to the wavelength [38] to experimentally access the longitudinal polarization component. Using an additional strong static magnetic field parallel to the optical axis and tuning the light field to resonantly drive a  $\pi$  transition allows the selective coupling of the longitudinal polarization only. To separate the  $\pi$  transition from the  $\sigma^\pm$  transitions beyond Doppler broadening (roughly 0.5 GHz at 100°C), we need a sufficiently large magnetic field (roughly  $B \sim 1$  T). For such large magnetic fields, isolated pure  $\pi$  transitions exist, e.g., from  $|5S_{1/2} m_j m_l\rangle = |5S_{1/2} \pm 1/2 \pm 3/2\rangle$  to  $|5P_{3/2} \pm 1/2 \pm 3/2\rangle$ . This method of light-matter coupling can, however, be extended to more general settings, where the angle of the magnetic field can be tuned and thus different components of vectorial topological light can be superposed and inscribed into matter.

In conclusion, we have presented a simple algorithm to realize an arbitrary (sufficiently well-behaved) field in the focal plane in the longitudinal polarization component and elaborated on how to realize the transverse components for it. We have highlighted the importance of the occurrence of evanescent waves and discussed the important degrees of freedom in the choice of the transverse polarization components. Using this method has the potential to broaden the range of possible vectorial structured light fields extensively and lead to a range of applications in various fields in physics, including nonlinear optics and Bose-Einstein condensates.

The authors would like to thank the referees for their careful reading and suggestions. F. M. acknowledges useful discussions with D. Dorigoni. This work is funded by the Leverhulme Trust Research Program Grant No. RP2013-K-009, SPOCK: Scientific Properties of Complex Knots. S. S. acknowledges support by the Qatar National Research Fund (Grant No. NPRP 8-246-1-060).

- 
- [1] M. Born, E. Wolf, and A. Bhatia, *Principles of Optics: Electromagnetic Theory of Propagation, Interference and Diffraction of Light* (Cambridge University Press, Cambridge, England, 1999).
  - [2] B. Richards and E. Wolf, *Proc. R. Soc. A* **253**, 358 (1959).
  - [3] K. S. Youngworth and T. G. Brown, *Opt. Express* **7**, 77 (2000).
  - [4] H. Wang, L. Shi, B. Lukyanchuk, C. Sheppard, and C. T. Chong, *Nat. Photonics* **2**, 501 (2008).
  - [5] S. Quabis, R. Dorn, M. Eberler, O. Glöckl, and G. Leuchs, *Opt. Commun.* **179**, 1 (2000).
  - [6] R. Dorn, S. Quabis, and G. Leuchs, *Phys. Rev. Lett.* **91**, 233901 (2003).
  - [7] C. Hnatovsky, V. Shvedov, W. Krolikowski, and A. Rode, *Phys. Rev. Lett.* **106**, 123901 (2011).
  - [8] T. Bauer, P. Banzer, E. Karimi, S. Orlov, A. Rubano, L. Marrucci, E. Santamato, R. W. Boyd, and G. Leuchs, *Science* **347**, 964 (2015).
  - [9] L. Allen, M. W. Beijersbergen, R. J. C. Spreeuw, and J. P. Woerdman, *Phys. Rev. A* **45**, 8185 (1992).
  - [10] J. F. Nye, *Natural Focusing and Fine Structure of Light: Caustics and Wave Dislocations* (Institute of Physics, Bristol, 1999).
  - [11] *Structured Light and Its Applications*, edited by D. L. Andrews (Academic, New York, 2008).
  - [12] H. Rubinsztein-Dunlop *et al.*, *J. Opt.* **19**, 013001 (2017).
  - [13] S. Franke-Arnold and N. Radwell, *Opt. Photonics News* **28**, 28 (2017).
  - [14] F. Maucher, T. Pohl, S. Skupin, and W. Krolikowski, *Phys. Rev. Lett.* **116**, 163902 (2016).
  - [15] R. W. Gerchberg and W. O. Saxton, *Optik* **35**, 237 (1972).
  - [16] D. G. Grier, *Nature (London)* **424**, 810 (2003).
  - [17] G. Whyte and J. Courtial, *New J. Phys.* **7**, 117 (2005).
  - [18] E. R. Shanblatt and D. G. Grier, *Opt. Express* **19**, 5833 (2011).
  - [19] J. F. Nye, *Proc. R. Soc. A* **387**, 105 (1983).

- [20] M. V. Berry and M. R. Dennis, *Proc. R. Soc. A* **457**, 2251 (2001).
- [21] J. Leach, M. R. Dennis, J. Courtial, and M. J. Padgett, *New J. Phys.* **7**, 55 (2005).
- [22] M. R. Dennis, R. P. King, B. Jack, K. O'Holleran, and M. J. Padgett, *Nat. Phys.* **6**, 118 (2010).
- [23] S. J. Tempone-Wiltshire, S. P. Johnstone, and K. Helmerson, *Sci. Rep.* **6**, 24463 (2016).
- [24] H. K. Moffatt, *J. Fluid Mech.* **35**, 117 (1969).
- [25] H. K. Moffatt, *Nature (London)* **347**, 367 (1990).
- [26] D. Kleckner and W. T. M. Irvine, *Nat. Phys.* **9**, 253 (2013).
- [27] P. M. Sutcliffe and A. T. Winfree, *Phys. Rev. E* **68**, 016218 (2003).
- [28] F. Maucher and P. Sutcliffe, *Phys. Rev. Lett.* **116**, 178101 (2016).
- [29] F. Maucher and P. Sutcliffe, *Phys. Rev. E* **96**, 012218 (2017).
- [30] U. Tkalec, M. Ravnik, S. Copar, S. Zumer, and I. Musevic, *Science* **333**, 62 (2011).
- [31] A. Martinez, M. Ravnik, B. Lucero, R. Visvanathan, S. Zumer, and I. I. Smalyukh, *Nat. Mater.* **13**, 258 (2014).
- [32] M. Lax, W. H. Louisell, and W. B. McKnight, *Phys. Rev. A* **11**, 1365 (1975).
- [33] F. Maucher, S. A. Gardiner, and I. G. Hughes, *New J. Phys.* **18**, 063016 (2016).
- [34] J. W. Goodman, *Introduction to Fourier Optics*, 3rd ed. (Roberts, Englewood, CO, 2016).
- [35] J. Ruostekoski and Z. Dutton, *Phys. Rev. A* **72**, 063626 (2005).
- [36] L. Novotny, M. R. Beversluis, K. S. Youngworth, and T. G. Brown, *Phys. Rev. Lett.* **86**, 5251 (2001).
- [37] G. F. Quinteiro, F. Schmidt-Kaler, and C. T. Schmiegelow, *Phys. Rev. Lett.* **119**, 253203 (2017).
- [38] A. Sargsyan, A. Papoyan, I. G. Hughes, C. S. Adams, and D. Sarkisyan, *Opt. Lett.* **42**, 1476 (2017).